Chapter 32

Weak PING rhythms

In the PING model of Chapter 30, each E-cell and each I-cell fires once on each cycle of the oscillation. This is not what is usually seen experimentally in gamma rhythms. Much more typically, each participating pyramidal cells fires on some, but not all population cycles. The same is true for the participating inhibitory interneurons, although they usually participate on a larger proportion of population cycles. Figure 32.1 reproduces a small part of [33, Fig. 1] to illustrate this point. In the experiment underlying [33, Fig. 1], the gamma oscillations were induced by application of *kainate*, which activates glutamate receptors called the *kainate receptors*. This sort of oscillations can persist for very long times in the *in vitro* preparation (on the order of hours), and are therefore called *persistent gamma oscillations* [21, 32].

We call PING-like models in which the E-cells participate "sparsely", i.e., on a fraction of the population cycles only, *weak PING* models. By contrast, we will refer to the models of Chapter 30 as *strong PING* models. One way of obtaining weak PING oscillations is to make the drive to the E-cells stochastic [10]. In such a model, each individual E-cell participates only on those population cycles on which it happens to have sufficient drive. We refer to this as *stochastic weak PING*. A far more detailed stochastic model of gamma rhythms with sparse participation of the E-cells is due to Roger Traub; see for instance [156]. In Traub's model, individual model neurons have multiple compartments. The gamma rhythm is driven by stochastic activity originating in the pyramidal cell axons and amplified by axo-axonal gap junctions. One can think of the stochastic weak PING model studied here as a very much simplified caricature of Traub's model.

An alternative way of obtaining sparse participation of E-cells is to add adaptation currents to the E-cell model, which can prevent individual E-cells from firing at or even near gamma frequency [88, 97, 109]. We call this *adaptation-based weak PING*. We illustrate the stochastic and adaptation-based weak PING mechanisms with numerical examples in Sections 32.1 and 32.2, and discuss differences in their properties.

LeMasson and Kopell [93] proposed an *h-current-based weak PING* mecha-

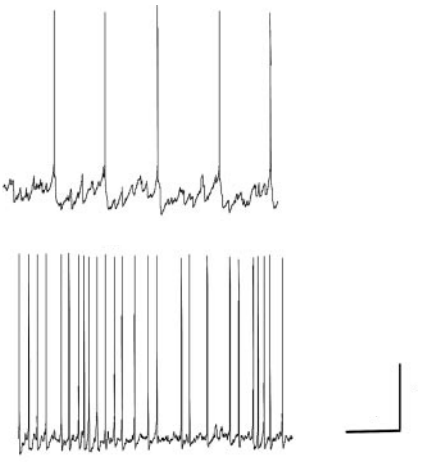

Figure 32.1. *Two voltage traces from Fig. 1 of [33]. These are recordings from a slice of rat auditory cortex. Gamma oscillations are induced by applying kainate. Fast-firing interneurons fire on almost every gamma cycle (bottom trace), while pyramidal cells fire sparsely (top trace). Scale bars: 200 ms and 25 mV. Reproduced with publisher's permission.*

nism. In their model, each E-cell has an h-current that builds up as the cell is hyperpolarized by the activity of the I-cells, until it reaches a level that forces a spike of the E-cell. Abstractly, adaptation-based and h-current-based weak PING are similar. In the former, a hyperpolarizing current is activated by firing, then gradually decays in the absence of firing; in the latter, a depolarizing current is inactivated by firing, then gradually recovers in the absence of firing.

32.1 Stochastic weak PING

We begin with the code generating Fig. 30.4. We reduce the mean external drive $\overline{I}_E$, but instead each E-cell now receives a sequence of brief excitatory synaptic input pulses, modeled as in Section 20.2, with parameters $\tau_{r,E}$, $\tau_{\text{peak},E}$, $\tau_{d,E}$, and $v_{\text{rev},E}$ as in Section 30.2. These pulses arrive on a Poisson schedule with mean frequency f_{stoch}. The Poisson schedules for different E-cells are independent of each other, and are discretized as described in Appendix C.11, with the time step Δt used to integrate the differential equations.

We will describe explicitly what this means. Focus on a single E-cell. Associated with this cell, there is a variable q_{stoch}. In each time step, this variable decays according to the differential equation

$$\frac{dq_{stoch}}{dt} = -\frac{q_{stoch}}{\tau_{d,q,E}}, \tag{32.1}$$

where $\tau_{d,q,E}$ is set so that $\tau_{\text{peak},E}$ has the desired value (we always use $\tau_{\text{peak},E} = 0.5\,\text{ms}$, as in Chapter 30). We discretize all differential equations using the midpoint method, even eq. (32.1), which we could of course also solve analytically. At the end of the time step, q_{stoch} jumps to 1 with probability (see eq. (C.30))

$$\frac{f_{stoch}}{1000}\,\Delta t.$$

The jumps in the variables q_{stoch} associated with different E-cells are independent of each other. A second variable associated with each E-cell is the synaptic gating variable s_{stoch}. It satisfies (see eq. (20.7))

$$\frac{ds_{stoch}}{dt} = q_{stoch}\frac{1 - s_{stoch}}{\tau_{r,E}} - \frac{s_{stoch}}{\tau_{d,E}}.$$

The stochastic input to the E-cell is then (see eq. (20.8))

$$I_{stoch} = \overline{g}_{stoch} s_{stoch}\,(v_{\text{rev},E} - v)\,,$$

where $\overline{g}_{stoch} > 0$.

One other detail of the simulations deserves mention: As discussed in Section 24.1, we initialize each E-cell at a random phase, uniformly distributed between 0 and 1, on its limit cycle. The initialization takes into account the deterministic external drive, but *not* the stochastic external drive.

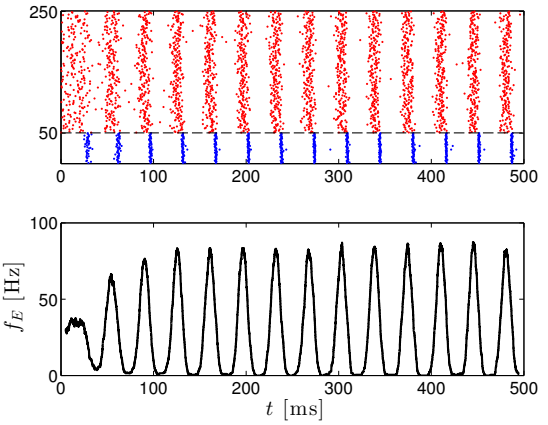

Figure 32.2. *Upper panel: Like upper panel of Fig. 30.4, but $\overline{I}_E$ has been reduced from 1.4 to 0.5, and instead the E-cells are driven by Poisson sequences of excitatory synaptic input pulses. The parameters characterizing the stochastic input are $f_{\text{stoch}} = 60$, $\overline{g}_{\text{stoch}} = 0.03$. Lower panel: Time-dependent mean firing frequency of E-cells, as defined in eq. (32.2). The overall mean firing frequencies of the E- and I-cells (see eq. (32.3)) are $\hat{f}_E \approx 27.4$ Hz and $\hat{f}_I \approx 27.0$ Hz.* [POISSON_PING_1]

Our goal is to set parameters so that participation of the E-cells is sparse — the mean firing frequency of an E-cell should be much below that of an I-cell.

At any given time, most E-cells will be near rest. Therefore plotting the average membrane potential of the E-cells, as we did in most of the figures of Chapter 30, is not the best way of displaying the rhythmicity that emerges in the network here. We plot instead the *time-varying mean firing frequency*, $f_E = f_E(t)$, of the E-cells, which we define as follows.

$$f_E(t) = 1000 \times \frac{\text{number of spikes of E-cells in interval } [t-5, t+5]}{10 N_E}. \qquad (32.2)$$

For t within less than 5 ms of the start or the end of the simulation, we leave $f_E(t)$ undefined. The factor of 1000 in eq. (32.2) is needed because we measure time in ms, but frequency in Hz. Finally, we also define the *overall mean firing frequencies*, $\hat{f}_E$ and $\hat{f}_I$, of the E- and I-cells. The definition of $\hat{f}_E$ is

$$\hat{f}_E = 1000 \times \frac{\text{number of spikes of E-cells overall}}{\text{time simulated (in ms)} \times N_E}, \qquad (32.3)$$

and the definition of $\hat{f}_I$ is analogous. We want to set parameters so that the E-cells have mean firing frequencies far below those of the I-cells, so $\hat{f}_E \ll \hat{f}_I$.

Figure 32.2 shows results of a first network simulation. There is a very clean oscillation visible in Fig. 32.2, but it is a bit slow for a gamma oscillation (below 30 Hz), and the E- and I-cells fire at approximately equal mean frequencies, once per population cycle. To reduce the E-cell participation rate, we raise the excitability of the I-cells, by increasing $\overline{I}_I$ from 0 to 0.8. This should cause the I-cell spike volleys to be triggered more quickly, aborting some of the E-cell spiking activity. Indeed that is precisely what happens; see Fig. 32.3, where the E-cells participate on fewer than every second population cycle, on the average: $\hat{f}_E \approx 16.3$ Hz, $\hat{f}_I \approx 39.6$ Hz. ($\hat{f}_I$ is approximately the frequency of the population rhythm.)

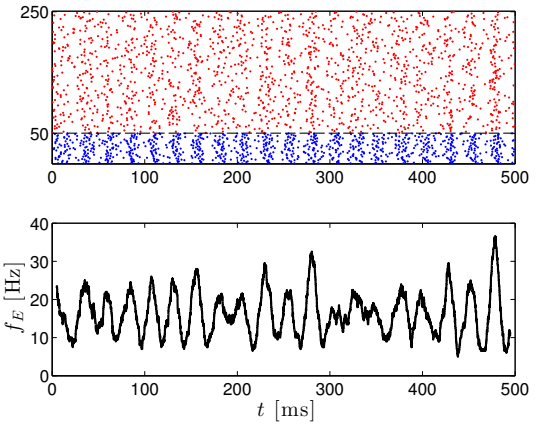

Figure 32.3. *Like Fig. 32.2, but with* $\overline{I}_I = 0.8$, $\sigma_I = 0.05$. *Now the overall mean firing frequencies are* $\hat{f}_E \approx 16.3$ *Hz,* $\hat{f}_I \approx 39.6$ *Hz.* [POISSON_PING_2]

How changes in the network parameters affect stochastic weak PING is not satisfactorily understood at the present time. However, not surprisingly, sparseness

of E-cell firing is promoted by factors that make inhibitory feedback faster and more effective. Such factors include large $\overline{I}_I$ (but not too large, so that the I-cells still fire only in response to E-cell activity), large $\hat{g}_{EI}$ and $\hat{g}_{IE}$, and small $\hat{g}_{II}$ (yet still large enough to keep the I-cells from firing without being prompted by the E-cells). Figure 32.4 shows an example in which I deliberately chose parameters to make E-cell firing sparse. I left out all network heterogeneity in this example, to make sure that $\hat{f}_E$ is not affected by *suppression* of E-cells with low external drive, but only by *cycle skipping* resulting from random lulls in the Poisson sequence of excitatory input pulses. Individual E-cells participate on approximately every fifth population cycle on the average in Fig. 32.4.

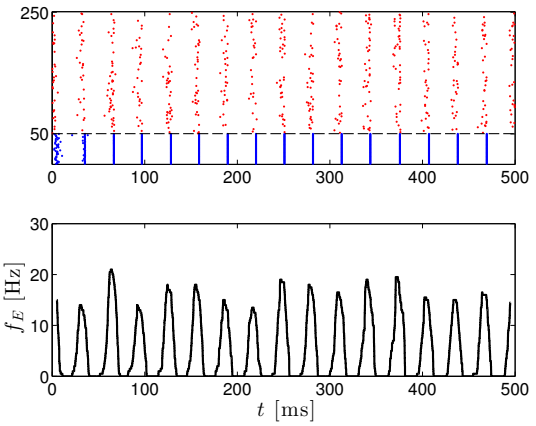

Figure 32.4. *Spike rastergram of a stochastically driven weak PING network (top), and time-dependent mean firing frequency of the E-cells (bottom). The parameters are* $N_E = 200$, $N_I = 50$, $\overline{I}_E = 0.6$, $\sigma_E = 0$, $\overline{I}_I = 0.6$, $\sigma_I = 0$, $\hat{g}_{EE} = 0$, $\hat{g}_{EI} = 1.25$, $\hat{g}_{IE} = 1.25$, $\hat{g}_{II} = 0.4$, $p_{EI} = 1$, $p_{IE} = 1$, $p_{II} = 1$, $\tau_{r,E} = 0.3$, $\tau_{\text{peak},E} = 0.3$, $\tau_{d,E} = 3$, $v_{\text{rev},E} = 0$, $\tau_{r,I} = 0.3$, $\tau_{\text{peak},I} = 0.3$, $\tau_{d,I} = 9$, $v_{\text{rev},I} = -75$, $f_{\text{stoch}} = 40$, $g_{\text{stoch}} = 0.1$. *Here the overall mean frequency of the E-cells is* $\hat{f}_E \approx 5.7$ *Hz, and that of the I-cells is* $\hat{f}_I \approx 31.7$ *Hz.* [POISSON_PING_3]

It is interesting to plot a single E-cell voltage trace; see Fig. 32.5. (I intentionally picked one that fires four spikes in the simulated time interval; most fire fewer than four.) When comparing with the upper trace of Fig. 32.1, you will see significant differences. In particular, the firing of the pyramidal cell in Fig. 32.1 is fairly regular, while in Fig. 32.5, the inter-spike intervals vary greatly. Also, the pyramidal cell in Fig. 32.1 has a rising membrane potential between spikes (with fluctuations superimposed), whereas the voltage trace in Fig. 32.5 shows oscillations around a roughly constant mean between spikes. Both of these discrepancies could be explained by an adaptation current, brought up by firing and gradually decaying between spikes. We will next consider networks in which there is such an adaptation current in the E-cells.

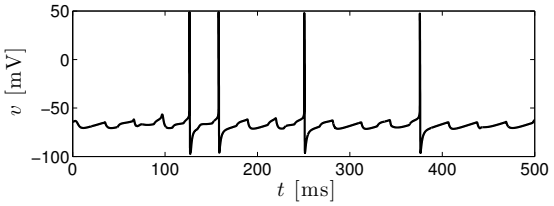

Figure 32.5. *Voltage trace of one of the E-cells in Fig. 32.4.* [POISSON_PING_3_VOLTAGE_TRACE]

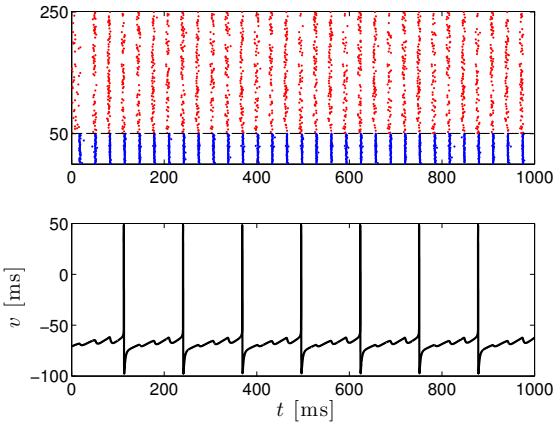

Figure 32.6. *Spike rastergram of a PING network with an M-current in the E-cells (top), and voltage trace of one of the E-cells (bottom). The parameters are* $N_E = 200$, $N_I = 50$, $\overline{I}_E = 3.0$, $\sigma_E = 0.05$, $\overline{I}_I = 0.7$, $\sigma_I = 0.05$, $\hat{g}_{EE} = 0$, $\hat{g}_{EI} = 0.5$, $\hat{g}_{IE} = 0.5$, $\hat{g}_{II} = 0.5$, $p_{EI} = 0.5$, $p_{IE} = 0.5$, $p_{II} = 0.5$, $\tau_{r,E} = 0.5$, $\tau_{\text{peak},E} = 0.5$, $\tau_{d,E} = 3$, $v_{\text{rev},E} = 0$, $\tau_{r,I} = 0.5$, $\tau_{\text{peak},I} = 0.5$, $\tau_{d,I} = 9$, $v_{\text{rev},I} = -75$, $\overline{g}_{\text{M}} = 1.0$. *The overall mean frequency of E-cells is* $\hat{f}_E \approx 10$ *Hz, and that of the I-cells is* $\hat{f}_I \approx 29$ *Hz.* [M_CURRENT_PING_1]

32.2 Adaptation-based, deterministic weak PING

Again we begin with the code generating Fig. 30.4. We add to the E-cells the model M-current of Section 9.1. We take the maximum conductance $\overline{g}_{\text{M}}$ to be the same for all E-cells. We initialize each E-cell at a random phase, uniformly distributed between 0 and 1, on its limit cycle. The M-current is considered part of the neuronal model, so it is turned on during the preliminary calculation that initializes the E-cells. Because the M-current is active even in the absence of firing (see Section 9.1), we must raise the drive to the E-cells to maintain a gamma frequency rhythm. As in Section 32.1, sparseness of E-cell firing is promoted by making the inhibitory feedback loop more responsive and more effective: We take $\overline{I}_I$ to be larger than in Fig. 30.4, and we double $\hat{g}_{EI}$ and $\hat{g}_{IE}$, in comparison with the simulation of Fig.

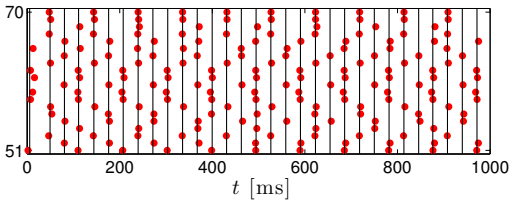

Figure 32.7. *Closeup of the rastergram in Fig. 32.6, showing only the spike times of the first 20 E-cells. The vertical lines indicate "local maxima of the overall E-cell firing rate". (For the precise definition of that, consult the Matlab code that generates the figure.)* [M_CURRENT_PING_1_CLOSEUP]

30.4. We also double $\hat{g}_{II}$, but for a different reason: With our parameter choices as described so far, some I-cells fire without being prompted by an E-cell spike volley. Raising $\hat{g}_{II}$ prevents this. Figure 32.6 shows a simulation with these parameter choices. In two regards, there appears to be a better match with Fig. 32.1 in Fig. 32.6 than in Fig. 32.5: There is now an upward trend between spikes (although a slight one), and the firing of the E-cell is regular, just much slower than the population rhythm.

A closer look at the rastergram reveals — not surprisingly, considering the regularity of the voltage trace in Fig. 32.6 — approximate *clustering* of the E-cell action potentials. Figure 32.7 is a close-up of Fig. 32.6, and demonstrates the clustering. The spiking pattern is shown for 20 E-cells in Fig. 32.7, cells 51 through 70 in the network. (Cells 1 through 50 are I-cells.) Some E-cells fire on one out of three population cycles, others on one out of four, and some cells toggle between these two patterns.

Shortening the decay time constant of inhibition in Fig. 32.6, while leaving all other parameters unchanged, results in a higher population frequency, but in similar E-cell firing rates, and therefore sparser E-cell participation, i.e., more clusters; see Fig. 32.8. Shortening the decay time constant of adaptation (here, of the M-current), while leaving all other parameters unchanged, results in a slight increase in the population frequency, but in a substantial increase in the E-cell firing rate, and therefore less sparse E-cell participation, i.e., fewer clusters; see Fig. 32.9. The population fires another volley as soon as inhibition falls to a sufficiently low level, while an individual cell fires another action potential as soon as its adaptation (M-current) falls to a sufficiently low level. For detailed analyses of the parameter dependence of the number of clusters and the population frequency in adaptation-based weak PING, see [88] and [97].

For the parameters of Fig. 32.6, the clustered solution shown in the figure is not the only possible clustered solution. In particular, if all cells are initialized approximately equally, there will be one dominating cluster, much larger than the others. To demonstrate this, assume that for $-200 \leq t \leq 0$, the drive $\overline{I}_E$ and $\overline{I}_I$ are zero, with all other parameters as in Fig. 32.6. By time $t = 0$, all cells then come to rest to very good approximation, regardless of how they are initialized at

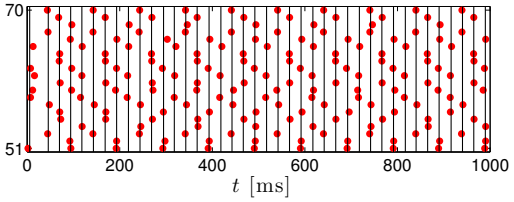

Figure 32.8. *Same as Fig. 32.7, but with* $\tau_{d,I} = 4.5$. *The overall mean frequency of E-cells is* $\hat{f}_E \approx 10$ *Hz, and that of the I-cells is* $\hat{f}_I \approx 38$ *Hz.* [M_CURRENT_PING_2_CLOSEUP]

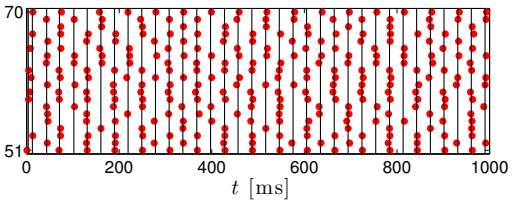

Figure 32.9. *Same as Fig. 32.7, but with the decay time constant of the M-current halved. The overall mean frequency of E-cells is* $\hat{f}_E \approx 15$ *Hz, and that of the I-cells is* $\hat{f}_I \approx 33$ *Hz.* [M_CURRENT_PING_3_CLOSEUP]

time $t = -200$. Assume that at time $t = 0$, $\overline{I}_E$ is raised to 3.0, and $\overline{I}_I$ to 0.7, the values of Fig. 32.6. The result is shown in Fig. 32.10. There are three clusters — two smaller ones, and a dominating one of approximately twice the size of the two smaller ones.

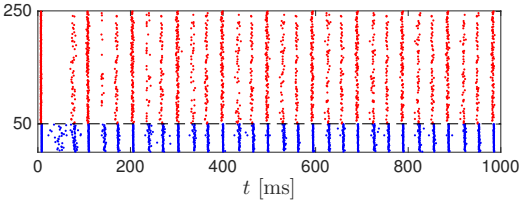

Figure 32.10. *Simulation as in Fig. 32.6, but with all cells starting at time* 0 *from the equlibrium positions corresponding to* $\overline{I}_E = \overline{I}_I = 0$.
[M_CURRENT_PING_1_FROM_REST]

32.3 Deterministic weak PING without any special currents

We saw that in ING clustering is possible (although fragile) with just the spike-generating sodium and delayed rectifier potassium currents; see Section 31.4. Is the same true in PING? The answer is yes. An example is shown in Fig. 32.11. However, the parameters here seem unlikely to be biologically realistic; the E-to-I synapses are extremely strong in fast, in order to generate very rapid inhibitory feedback. I have not been able to find find a similar example with biologically more plausible parameters.

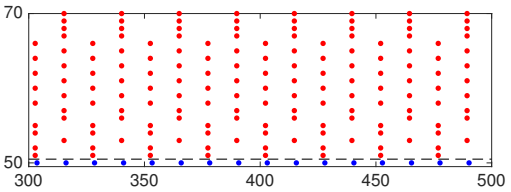

Figure 32.11. *Spike rastergram of a PING network with* $N_E = 200$, $N_I = 50$, $\overline{I}_E = 1.4$, $\sigma_E = 0$, $\overline{I}_I = 0.2$, $\sigma_I = 0$, $\hat{g}_{EE} = 0$, $\hat{g}_{EI} = 5$, $\hat{g}_{IE} = 0.25$, $\hat{g}_{II} = 0.75$, $p_{EI} = 1$, $p_{IE} = 1$, $p_{II} = 1$, $\tau_{r,E} = 0.05$, $\tau_{\text{peak},E} = 0.05$, $\tau_{d,E} = 1$, $v_{\text{rev},E} = 0$, $\tau_{r,I} = 0.1$, $\tau_{\text{peak},I} = 0.1$, $\tau_{d,I} = 9$, $v_{\text{rev},I} = -75$. *Only the last 200 ms of a 500 ms simulation and only spike times of one of the I-cells and 20 of the E-cells are shown.* [PING_CLUSTERS]

We will discuss clustering in PING networks without adaptation in a more theoretical way using what is arguably the simplest possible PING-like network: Two identical LIF neurons, with membrane potentials v_1 and v_2, governed by

$$\frac{dv_1}{dt} = -\frac{v_1}{\tau_m} + I - g_I s(t) v_1 \quad \text{for } v_1 < 1, \tag{32.4}$$

$$\frac{dv_2}{dt} = -\frac{v_2}{\tau_m} + I - g_I s(t) v_2 \quad \text{for } v_2 < 1, \tag{32.5}$$

$$\frac{ds}{dt} = -\frac{s}{\tau_I} \quad \text{for } v_1 < 1 \text{ and } v_2 < 1, \tag{32.6}$$

$$v_1(t+0) = 0 \quad \text{if } v_1(t-0) = 1, \tag{32.7}$$

$$v_2(t+0) = 0 \quad \text{if } v_2(t-0) = 1, \tag{32.8}$$

$$s(t+0) = 1 \quad \text{if } v_1(t-0) = 1 \text{ or } v_2(t-0) = 1. \tag{32.9}$$

We assume drive above the firing threshold: $\tau_m I > 1$. We refer to the two LIF neurons as the *E-cells*. The firing of one E-cell is assumed to trigger an inhibitory response. There are no I-cells explicitly included in this model, but the effect of the inhibitory population is represented by the gating variable s, assumed to be raised to its maximum value 1 in response to firing of one of the two E-cells.

We note that our model system differs from a system of two LIF neurons coupled by inhibitory synapses: Here there is only one single gating variable s,

affecting both neurons equally. In a network of two LIF neurons with inhibitory coupling, there would be two different gating variables, s_1 and s_2.

We refer to a solution of (32.4)–(32.9) as a *cluster solution* if the firing of the two E-cells alternates. We call a cluster solution *anti-synchronous* if the firing of the first E-cell always occurs exactly in the middle of the interspike interval of the second E-cell, and vice versa.

To study phase-locking in our system, we assume that the first E-cell fires at time 0, so $v_1(0+0) = 0$ and $s(0+0) = 1$. We use the letter x to denote $v_2(0+0)$, and assume $0 < x < 1$. We denote by T_1 the smallest positive time with $v_2(T_1 - 0) = 1$, and define $\psi(x) = v_1(T_1)$. We record some simple properties of the function ψ in the following proposition; compare Fig. 32.12.

Proposition 32.1. *(a) The function $\psi = \psi(x)$, $0 < x < 1$, is strictly decreasing and continuous, with $0 < \psi(x) < 1$ and $\lim_{x \searrow 0} \psi(x) = 1$. (b) The limit $\lim_{x \nearrow 1} \psi(x)$ equals 0 if $0 \le g_I \le I - 1/\tau_m$, and lies strictly between 0 and 1 if $g_I > I - 1/\tau_m$.*

Proof. Exercise 4. □

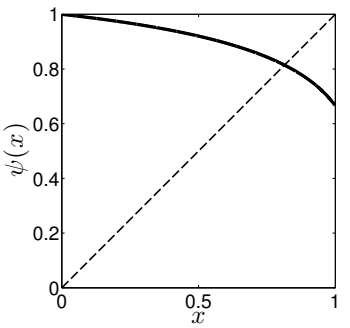

Figure 32.12. *The function ψ defined in this section, for $\tau_m = 10$, $I = 0.12$, $g_I = 0.05$, $\tau_I = 5$.* [PLOT_PSI]

We denote by T_2 the smallest positive time with $v_1(T_2 - 0) = 1$, and define $\phi(x) = v_2(T_2)$. For all $x \in (0, 1)$,

$$\phi(x) = \psi(\psi(x)) \tag{32.10}$$

(see exercise 5). For the parameters of Fig. 32.12, the graph of ϕ is shown in Fig. 32.13. In words, if the first E-cells fires, and the second E-cell is at membrane potential $x \in (0, 1)$, then the next time when the first E-cell fires, the second E-cell will be at membrane potential $\phi(x) \in (0, 1)$.

The limits of ψ and ϕ as $x \searrow 0$ or $x \nearrow 1$ exist by Proposition 32.1. We denote them by $\psi(0)$, $\psi(1)$, $\phi(0)$, and $\phi(1)$. There is a possible point of confusion here, which we will address next. Note that in Fig. 32.13, $\phi(0)$ is not zero. In fact, Proposition 32.1 implies that $\phi(0) = 0$ if and only if $g_I \le I - 1/\tau_m$, and in Fig.

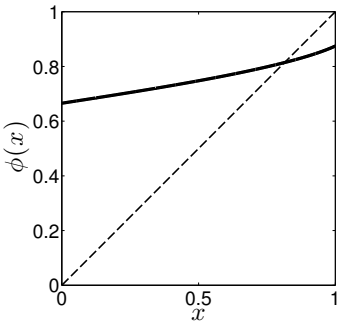

Figure 32.13. *The function ϕ defined in this section, for $\tau_m = 10$, $I = 0.12$, $g_I = 0.05$, $\tau_I = 5$.* [PLOT_PHI]

32.13, $g_I = 0.05 > I = 1/\tau_m = 0.02$. You might think that this should imply that perfect synchrony of the two E-cells is not a possibility. This is not correct. Perfect synchrony is always a possibility in this model. If the two E-cells fire at exactly the same time once, the feedback inhibition will affect them in exactly the same way, and they will therefore always fire in synchrony in the future. However, if they fire only in *approximate* synchrony, the one that fires earlier can very substantially delay the one that fires later. So $\phi(0) > 0$ does not imply that synchrony is impossible, but it does imply that synchrony is unstable.

The solution of (32.4)–(32.9) is a cluster solution if and only if $x = v_2(0+0)$ is a fixed point of ϕ, and an anti-synchronous solution if and only if x is a fixed point of ψ. The fixed point x_* in Fig. 32.13 is stable because $|\phi'(x_*)| < 1$; see Appendix B. It is the same as the fixed point in Fig. 32.12. It corresponds to the anti-synchronous solution, which is stable here.

In Figs. 32.12 and 32.13, one would have to choose $g_I \leq 0.02$ for $\psi(1)$ to become 0, and therefore $\phi(0)$ to become 0 and $\phi(1)$ to become 1. In Fig. 32.14, we show ψ and ϕ for the same parameters as in Figs. 32.12 and 32.13, but with g_I lowered to 0.015. Now $\phi(0) = 0$, but $\phi'(0) > 1$, and this implies that synchrony of the two E-cells is still unstable. The anti-synchronous solution is still stable.

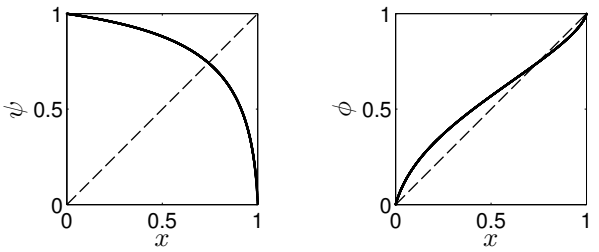

Figure 32.14. *The functions ψ and ϕ defined in this section, for $\tau_m = 10$, $I = 0.12$, $g_I = 0.015$, $\tau_I = 5$. Here g_I is so small that $\psi(1) = 0$, and therefore $\phi(0) = 0$ and $\phi(1) = 1$. Synchrony of the two E-cells is still unstable.* [PLOT_PSI_PHI]

This discussion suggests that in an E-I network with a very rapid inhibitory response, the E-cells will cluster, not synchronize. PING rhythms are possible only because the inhibitory response is *not* instantaneous. For instance, if a small delay between the firing of an E-cell and the inhibitory response (the reset of s to 1) is added to our model, synchrony becomes stable; see exercise 6.

Adaptation currents amplify the tendency towards clustering by holding back cells that are behind, since those cells have a stronger active adaptation current.

Exercises

32.1. (∗) In the simulation of Fig. 32.4, what happens if you double (a) f_{stoch}, or (b) g_{stoch}? How are $\hat{f}_E$ and $\hat{f}_I$ affected?

32.2. (∗) (†) Produce a figure similar to Fig. 32.4, but now using independent discrete Ornstein-Uhlenbeck processes (see eqs. (C.20)–(C.22) in Appendix C.6) in place of the independent Poisson sequences of excitatory input pulses used in Section 32.1. Note that this is different from what you did in exercise 30.7. There the same Ornstein-Uhlenbeck process was used for all neurons. Here the Ornstein-Uhlenbeck processes used for different neurons are independent of each other. Unlike the *global stochastic drive* in exercise 30.7, this sort of *cell-specific stochastic drive* cannot produce strongly varying population frequencies, but it can produce sparse participation of the E-cells.

32.3. (∗) How does Fig. 32.7 change (a) when $\hat{g}_{IE}$ is doubled, (b) when $\overline{g}_{\text{M}}$ is doubled?

32.4. (†) Prove Proposition 32.1.

32.5. Explain eq. (32.10).

32.6. (∗) In the code that generates Fig. 32.14, add a delay of 2ms between the firing of an E-cell and the inhibitory response. Show that this renders synchrony of the two E-cells stable, although anti-synchronous clustering remains stable.

32.7. (∗) (†) Generalize the model given by (32.4)–(32.9) to $N > 2$ LIF neurons, again with common feedback inhibition triggered immediately when just one of the LIF neurons fires. Initializing at random, does one typically obtain clustering, splay state solutions, or what else?